Computational Particle Mechanics
https://doi.org/10.1007/s40571-024-00747-6

Semi-empirical model for abrasive particle velocity prediction in abrasive waterjet based on momentum transfer efficiency

Hyun-Joong Hwang[1] · Yohan Cha[2] · Seok-Jun Kang[1] · Gye-Chun Cho[1]

Received: 8 January 2024 / Revised: 6 March 2024 / Accepted: 20 March 2024

Abstract

Abrasive waterjet (AWJ) is a technology that removes a target material with an abrasive accelerated by ultra-high-pressure water. Recently, its application for rock excavations in civil and geotechnical engineering has increased. AWJ excavation performance is affected by the abrasive velocity formed by momentum transfer during mixing and acceleration. The abrasive velocity varies owing to changes in the abrasive flow rate, focusing tube diameter, and focusing tube length. In this study, the momentum transfer efficiency (MTE) according to the abrasive flow rate and focusing tube geometry was investigated by a numerical analysis to better understand the multiphase flow inside the AWJ system. The MTE was defined based on the theoretical relationship between the abrasive velocity ratio and focusing tube factor, and evaluated through the empirical relationship between the water stiffness and focusing tube length. The optimal abrasive flow rate for generating efficient MTE was approximately 15 g/s, which enabled economical and effective acceleration of abrasive particles. Accordingly, a prediction model based on the derived MTE was developed for the final abrasive velocity generated at the tip of the focusing tube. Using the prediction model, it is possible to evaluate the comprehensive relationship between various AWJ parameters. Based on the prediction model, the abrasive–water flow ratio to generate the optimal abrasive velocity was 0.83. The developed prediction model provides guidelines for selecting the optimal focusing tube geometry and applying an economical abrasive flow rate when designing an AWJ system.

Keywords Abrasive waterjet · Abrasive particle velocity · Momentum transfer efficiency · Prediction model · CFD

List of symbols

A_o	Cross-sectional area of the orifice (mm^2)
C_d	Coefficient of discharge
C_D	Drag coefficient
D_a	Abrasive diameter (mm)
D_f	Focusing tube diameter (mm)
D_o	Orifice diameter (mm)
K	Water stiffness (mm^{-1})
L	Compressibility pressure characteristic (MPa)
L_f	Focusing tube length (mm)
$\dot{m}_a$	Abrasive flow rate (AFR) (g/s)
$\dot{m}_w$	Water flow rate (ml/s)
n	Compressibility constant
$p_{w,p}$	Water pump pressure (MPa)
v_a	Actual abrasive velocity (m/s)
$v_{a,id}$	Ideal abrasive velocity (m/s)
$v_{a,max}$	Maximum ideal abrasive velocity (m/s)
v_t	Terminal velocity (m/s)
$v_{w,id}$	Ideal water velocity (m/s)
$v_{w,o}$	Initial water velocity (m/s)
x	Distance along the focusing tube length (mm)
ζ	Focusing tube factor
ρ_w	Water density (kg/m^3)
ψ	Compressibility of water
ω	Abrasive velocity ratio

✉ Gye-Chun Cho
gyechun@kaist.edu

Hyun-Joong Hwang
hyunjoong@kaist.ac.kr

Yohan Cha
yohan@kaeri.re.kr

Seok-Jun Kang
incheon@kaist.ac.kr

[1] Department of Civil and Environmental Engineering, Korea Advanced Institute of Science and Technology (KAIST), Daejeon 34141, Republic of Korea

[2] Disposal Performance Demonstration R&D Division, Korea Atomic Energy Research Institute (KAERI), Daejeon 34057, Republic of Korea

Published online: 16 April 2024

AFR Abrasive flow rate (g/s)
MTE Momentum transfer efficiency

1 Introduction

Waterjet technology using ultra high-pressure water has been actively used in the fields of manufacturing, machining, and cleaning of materials such as metals, ceramics, and glass, because heat and stress are not generated around the target material being crushed [1, 20, 29, 48]. Recently, owing to the development of high-pressure pumps, waterjet technology has been actively applied in civil engineering, geotechnical engineering, and mining for materials such as rock and concrete [8, 24, 26]. This is because cutting and drilling in the desired shape is possible with simple manipulation of the operating parameters (e.g., water pump pressure, abrasive flow rate, or standoff distance) by an engineer, depending on the target material.

Waterjet technology can be classified into plain waterjet (PWJ) which uses only water, and abrasive waterjet (AWJ) which uses both abrasives and water. The former method employs the crushing of material by impacting the target material using the water pressure generated by a high-pressure pump. However, PWJ has limitations in crushing high-strength materials such as rocks. To solve this, material removal efficiency could be increased by adding abrasives to a PWJ [15, 17, 38]. AWJ technology is used in various fields and applied to materials ranging from soft materials, such as metals, to brittle materials, such as rock and concrete. In particular, to apply AWJs in geotechnical engineering, continuing research aims to reduce costs and increase rock excavation performance [2, 7, 12, 27, 35, 44]. However, in the case of AWJ cutting and drilling, the efficiency is reduced when applied to brittle materials compared with soft materials. Therefore, performance prediction for efficient rock excavation is essential. In particular, it is important to predict the momentum (i.e., abrasive velocity) of the abrasive produced in an AWJ system, because the momentum of the abrasive is the most important factor in rock excavation [13, 36].

Various AWJ parameters affect the momentum of the abrasive. Jegaraj and Babu [25] and Kechagias et al. [28] analyzed the dominant effect of the focusing tube diameter on the cutting width and surface roughness of the target material with AWJ performance. Hashish [18] experimentally investigated influence of the relationship between the focusing tube diameter and the water pump pressure on the optimal abrasive flow rate. Chalmers [9] conducted AWJ cutting experiments on the parameters of orifice diameter, abrasive flow rate, and focusing tube diameter, and found that the economically optimal focusing tube diameter is three times the orifice diameter. Because it is difficult for an engineer to directly observe the abrasive velocity using an AWJ system, various studies have been conducted to derive the abrasive velocity. Previous studies have mainly performed experimental and theoretical analyses to derive the abrasive velocity at the end of the focusing tube of an AWJ system. Balz et al. [3] measured the abrasive velocity and spatial location of an AWJ system using ultra-fast X-rays. Finally, the spatial position and velocity of the abrasive were experimentally analyzed through image post-processing using commercial software after capturing an image with a high-speed camera. In addition, the theoretical approaches proposed by Tazibt et al. [49], Hashish [19], and Cha et al. [5] were based on the conservation of momentum and energy law for water and abrasives. By setting the coordinates of the axial direction of the AWJ system, the water and abrasive velocities according to position can be expressed and calculated using equations. However, there is a limitation in that the theoretical expression for abrasive velocity is derived from a one-dimensional flow condition in the axial direction. Because the process of mixing water and abrasives is three-dimensional, it is necessary to derive a more accurate abrasive velocity.

It is challenging to theoretically induce the three-dimensional acceleration behavior of an abrasive in a fluid, because various physical quantities must be considered according to its location in space. In addition, it is difficult to experimentally obtain fluid flow information in an AWJ system, as it cannot be directly observed. The numerical approach to analyzing an AWJ system possesses the advantage of easily obtaining information regarding trends that are difficult to obtain theoretically and experimentally [11, 31, 50]. Deepak et al. [10] analyzed the effects of operating pressure and volume fraction on skin friction and exit kinetic energy in a focusing tube by performing a two-dimensional numerical analysis of an AWJ system. Hu et al. [23] modeled a two-dimensional AWJ based on the Eulerian–Lagrangian approach and analyzed the velocity and tracking of the abrasive inside the focusing tube through numerical analysis considering a two-phase flow (i.e., liquid and solid). Prisco and D'Onofrio [45] modeled a water jet based on the Eulerian–Eulerian approach in 3D and analyzed the jet velocity according to the spatial location in the water jet system.

Various studies have been conducted to determine the abrasive velocity at the tip of the focusing tube. However, the abrasive velocity considering three-phase flow (liquid, gas, and solid phases), and the comprehensive relationship between variables in three-dimensional space have not yet been derived. In this study, the effects of abrasive flow rate and focusing tube geometry (i.e., diameter and length) on abrasive velocity were analyzed through 3D numerical analysis, and the empirical expression for momentum transfer efficiency (MTE) were derived. In addition, according to

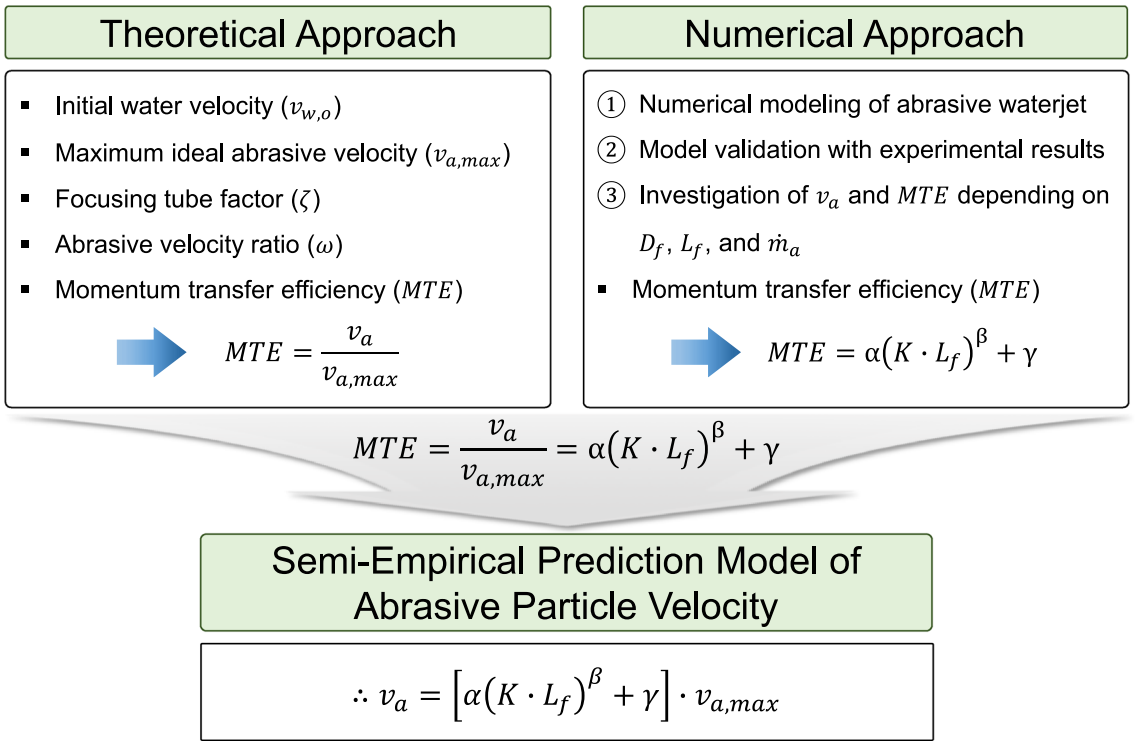

Fig. 1 Flow chart of semi-empirical model for abrasive particle velocity prediction

the theoretical equation based on the law of conservation of momentum, a prediction model for the abrasive velocity at the tip of the focusing tube was proposed using a comprehensive relationship with the MTE (Fig. 1). This work is expected to contribute to more accurate and efficient planning and design by utilizing prediction model that considers the operating parameters that engineers can easily apply and change using AWJ for rock excavation.

The remainder of this paper is organized as follows. Section 2 contains the theoretical background of AWJ mechanism. In Sect. 3, detailed information about the numerical method and model validation. Section 4 analyzes the results of the numerical simulations and discusses the semi-empirical prediction model. Finally, Sect. 5 presents the main findings of the research and provides some recommendations for future studies.

2 Theoretical background

The main energy source of an AWJ used in rock excavation is the momentum of the abrasive [36, 41, 43]. The mechanism of the AWJ system that accelerates the abrasive is illustrated in Fig. 2.

Water is delivered to the intensifier through a hydraulic pump, the pressure is increased, and the accumulator accumulates the high-pressure water. The generated high-pressure water is delivered to the orifice. High-pressure water is converted to high-speed water as it passes through a small-diameter orifice. Water is usually assumed to be an incompressible fluid; however, compressibility and discharge coefficient must be considered because AWJs create high-pressure conditions. According to Bernoulli's law, the initial water velocity ($v_{w,o}$) is expressed as [17, 39, 40]:

$$\begin{aligned} v_{w,o} &= C_d \cdot \psi \cdot \sqrt{\frac{2 \cdot p_{w,p}}{\rho_w}}, \\ \text{here, } C_d &= \frac{\dot{m}_w}{A_o \cdot \sqrt{2 \cdot \rho_w \cdot p_{w,p}}}, \\ \psi &= \sqrt{\frac{L}{p_{w,p} \cdot (1-n)}\left[\left(1 + \frac{p_{w,p}}{L}\right)^{1-n} - 1\right]}, \end{aligned} \tag{2.1}$$

where C_d is the coefficient of discharge, ψ is the compressibility of water, $p_{w,p}$ is the water pump pressure, ρ_w is the water density, $\dot{m}_w$ is the water flow rate, A_o is the cross-sectional area of the orifice, L is the compressibility pressure characteristic and n is the compressibility constant. In this study, the values $L = 300$ MPa and $n = 0.1368$ were adopted from Bridgman [4]. The initial water velocity is the primary energy source created by an AWJ system that is capable of accelerating abrasives.

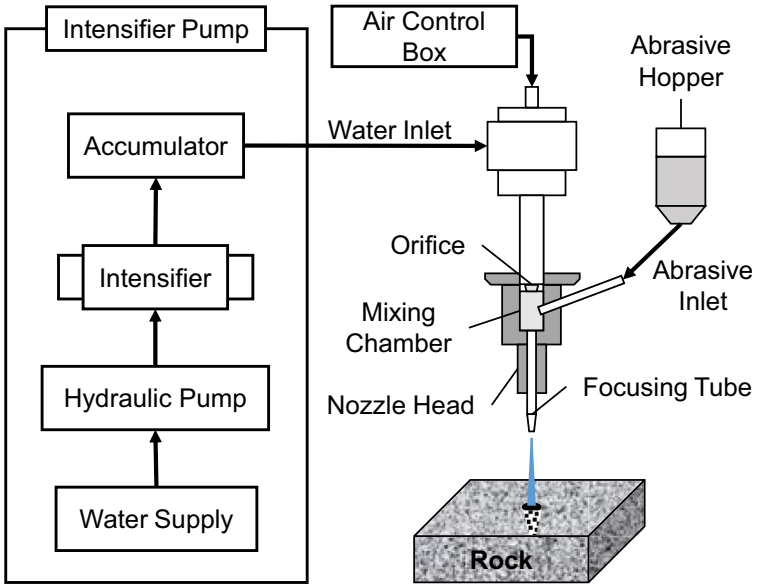

Fig. 2 Schematic of an abrasive waterjet (AWJ) system

The high-speed water generated through the orifice creates a Venturi suction effect, which introduces dry abrasives and air into the mixing chamber. The high-speed water and abrasives are mixed inside the mixing chamber, and the abrasives receive momentum from the water. The momentum balance equation from the momentum of water with an initial water velocity can be expressed as [17, 36, 37, 47]:

$$\dot{m}_w v_{w,o} = \dot{m}_w v_{w,id} + \dot{m}_a v_{a,id} = (\dot{m}_w + \dot{m}_a) v_t, \tag{2.2}$$

where $\dot{m}_a$ is the abrasive flow rate, $v_{w,id}$ is the ideal water velocity, $v_{a,id}$ is the ideal abrasive velocity, and v_t is the terminal velocity. Terminal velocity means that the velocities of the water and abrasive are the same. Theoretically, if complete momentum conservation is achieved without energy loss, the terminal velocity becomes the maximum ideal abrasive velocity ($v_{a,max}$), which is the maximum velocity that the abrasive can attain. It can be expressed as

$$v_{a,max} = \frac{v_{w,o}}{1 + \dot{m}_a/\dot{m}_w}. \tag{2.3}$$

The abrasive flow rate (AFR) and abrasive velocity are important parameters related to the kinetic energy of the abrasives. Previous studies have approached them theoretically to derive the abrasive velocity [5, 19]. Hashish [19] calculated the ideal abrasive velocity ($v_{a,id}$) according to the position of the focusing tube, as follows:

$$x = \frac{1}{K}\left[\frac{\zeta}{\zeta - 1} - ln\left(\frac{1}{1-\zeta}\right)\right], \quad \text{here,} \quad K = \frac{3C_D(1 + \dot{m}_a/\dot{m}_w)^2}{4D_o^2/D_f^2 \cdot D_a}, \quad \zeta = \frac{v_{a,id}}{v_{a,max}}, \tag{2.4}$$

where x is the distance along the focusing tube length, K is the water stiffness, ζ is the focusing tube factor, C_D is the drag coefficient, D_o is the orifice diameter, D_f is the focusing tube diameter, and D_a is the abrasive diameter.

In this study, the abrasive velocity ratio (ω) was defined as the ratio between the ideal abrasive velocity at the tip of the focusing tube and the actual abrasive velocity, given by:

$$\omega = \frac{v_a}{v_{a,id}}, \tag{2.5}$$

where v_a is the actual abrasive velocity and $v_{a,id}$ is the ideal abrasive velocity.

In addition, the momentum transfer efficiency (MTE) was defined as the ratio between the actual abrasive velocity (v_a) and the maximum ideal abrasive velocity ($v_{a,max}$), which can be calculated by multiplying the focusing tube factor (ζ) and the abrasive velocity ratio (ω), expressed as:

$$MTE = \zeta \cdot \omega = \frac{v_a}{v_{a,max}}. \tag{2.6}$$

If the actual abrasive velocity (v_a) can be determined directly through numerical analysis, then MTE can be calculated using the ratio of the maximum ideal abrasive velocity ($v_{a,max}$) derived from Eq. (2.3). In addition, because the MTE is related to the focusing tube factor (ζ), it can be expressed by assuming a power equation using the water stiffness (K) and focusing tube length (L_f), as follows:

$$MTE = \alpha\left(K \cdot L_f\right)^{\beta} + \gamma, \tag{2.7}$$

where α, β, and γ are empirically determined.

Therefore, by substituting Eq. (2.7) into Eq. (2.6), the actual abrasive velocity at the tip of the focusing tube can

be predicted:

$$\therefore v_a = MTE \cdot v_{a,max} = \left[\alpha\left(K \cdot L_f\right)^{\beta} + \gamma\right] \cdot v_{a,max}. \tag{2.8}$$

3 Numerical method

3.1 Numerical setup

The numerical simulation of the AWJ was performed using the ANSYS Fluent commercial software. This computational fluid dynamics (CFD) software analyzes fluid flow phenomena by discretizing and calculating the Navier–Stokes equations, which are nonlinear partial differential equations, based on the finite volume method (FVM) [14]. In this study, the ANSYS Fluent software was used to observe the abrasive velocity produced by the AWJ.

The AWJ flow consists of multiple phases. They can be divided into a continuous fluid phase, comprising air and water, and a discrete particle phase, such as abrasives. In this study, a volume of fluid (VOF) model was applied to implement a continuous fluid phase [22, 33, 42]. The VOF model analyzes multiphase flow using a surface-tracking technique when two or more phases exist on the basis of a fixed Eulerian mesh [21]. In the case of an AWJ, one equation of motion was equally applied to each phase, considering the free surface according to the interaction between air and water. The calculation was performed using only the volume fraction in the set grid. The air and water volume fractions in AWJ systems were 95 and 4%, respectively [49]. Therefore, the primary and secondary phases were applied with air and water, respectively. To observe the exact behavior of the abrasive, the simulation was set considering gravity. A standard k–epsilon turbulence model was applied to consider the viscosity between the phases [16, 30]. The input values of the standard k–epsilon turbulence model used in the numerical analysis are summarized in Table 1.

The discrete phase model (DPM) has been applied to implement discrete particle phases, such as abrasives [33, 34, 46]. The DPM model is a Lagrangian method for tracking and calculating particle trajectories. It calculates and tracks values such as mass, momentum, and energy along the trajectory when a particle moves within a set control volume. By calculating the influence between the fluid flow of the continuous phase and the particles of the dispersed phase, as mentioned previously, the fluid flow is continuously updated to perform iterative calculations. In addition, because particle trajectories can be changed by turbulence in fluid flow, the discrete random walk (DRW) model, a stochastic tracking method, was applied to consider the effect of turbulence. The DRW model is calculated considering flow characteristics, such as particle velocity, and is suitable for complex shapes, such as AWJ systems. In principle, the DPM model can be applied when the volume fraction occupied by particles is less than 10% of the total. In general, the volume fraction occupied by abrasives in AWJ systems is less than 10% [32, 49, 51].

Table 1 Input value of the constants in the standard k–epsilon model

σ_k	σ_ε	$C_{1\varepsilon}$	$C_{2\varepsilon}$	C_μ
1.0	1.3	1.44	1.92	0.09

The AWJ system was implemented as a three-dimensional model to analyze the behavior of abrasives in a three-dimensional space. Figure 3a shows the geometry of a simulation model in which water is injected from the top and passed through an orifice with a small diameter. In addition, the mixing chamber and abrasive inlet were configured such that the high-speed water passing through the orifice and abrasive could freely mix and transfer momentum. A simulation model was constructed to ensure that the water and abrasives mixed accordingly, passed through the focusing tube to obtain straightness, and spraying the water and abrasives from the tip. Figure 3b shows the specific locations of the applied variables when performing the numerical analysis.

The location and value of the boundary conditions applied to the simulation model of the AWJ are shown in Fig. 4. The water inlet pressure was set to 320 MPa. Additionally, because the VOF model was applied, the volume fraction of water was set to 1. The abrasive inlet was assigned a pressure of 101.325 kPa, considering the atmospheric pressure conditions. In general, the mechanism of the AWJ is due to the Venturi suction effect by high-speed water formed while passing through a small-diameter orifice. This effect introduces the abrasive material and air into the mixing chamber without additional external pressure. In addition, the volume fraction of water was set to zero, because it could not be introduced into the abrasive inlet. Because the outlet is where water and abrasives are sprayed into the air, a pressure of 101.325 kPa was set considering the atmospheric pressure conditions. The boundary condition acting on the wall was set as a reflection type to realize the collisions between the abrasive and the wall. To determine whether the numerical analysis converges, the attainment of convergence was assumed when the residuals of all physical quantities were less than 0.001, and the numerical analysis was terminated.

3.2 Model validation and cases

To verify this numerical model, the abrasive velocity results of Balz et al. [3] were compared with 14 simulation cases

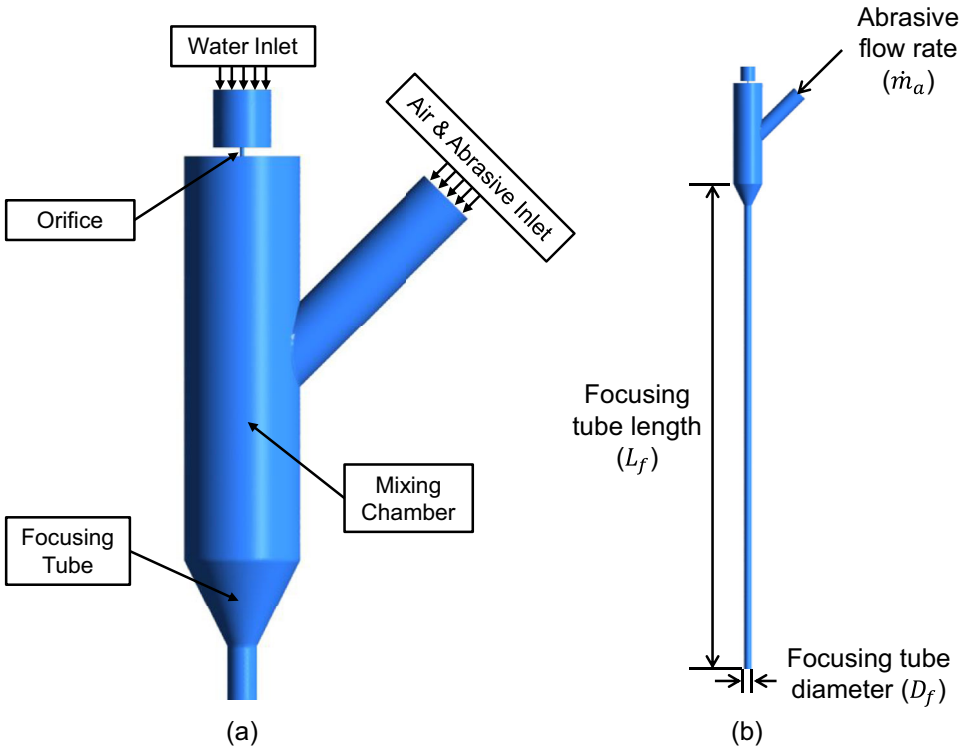

Fig. 3 Simulation model of abrasive waterjet system: **a** geometry and **b** simulation variables

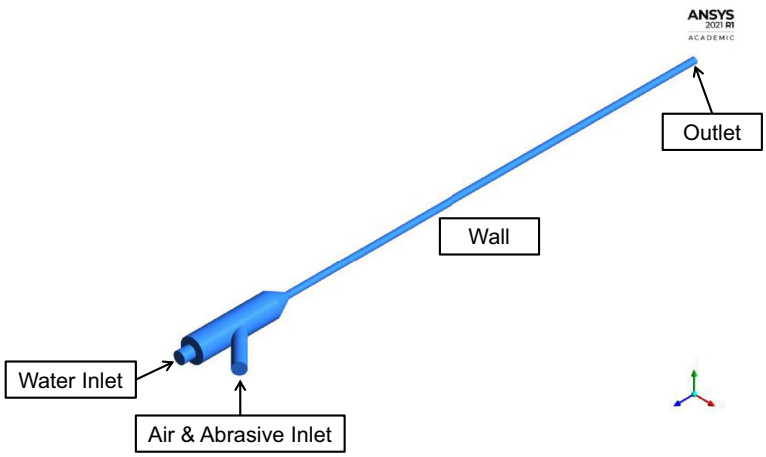

Fig. 4 Boundary condition position of the simulation model

from this study. For an accurate comparison, the AWJ specifications and input parameters were applied equally when performing the numerical analysis. For the AWJ system specification, an orifice diameter of 0.28 mm, focusing tube diameter of 0.80 mm, focusing tube length of 76 mm, and abrasive size of 0.20 mm were equally applied. In addition, for the input parameters, the water pump pressure, abrasive flow rate, and water flow rate were applied to 14 different cases. Figure 5 shows a graph comparing the abrasive velocity obtained through the numerical analysis and the experimental results; the results were found to be in significant agreement.

To explore the effects of abrasive flow rate and focusing tube geometry on abrasive velocity, different abrasive flow rates, focusing tube diameters, and focusing tube lengths were used in the numerical simulations. The numerical simulation cases are summarized in Table 2. A water pump pressure of 320 MPa, orifice diameter of 0.15 mm, and water flow rate of 10.67 ml/s were commonly applied in all numerical analysis cases. In addition, the abrasives were applied assuming a spherical shape with a diameter of 0.18 mm and a density of 3790 kg/m^3. Therefore, it was assumed that the drag coefficient (C_D) was 0.47 and the coefficient of discharge (C_d) was 0.755.

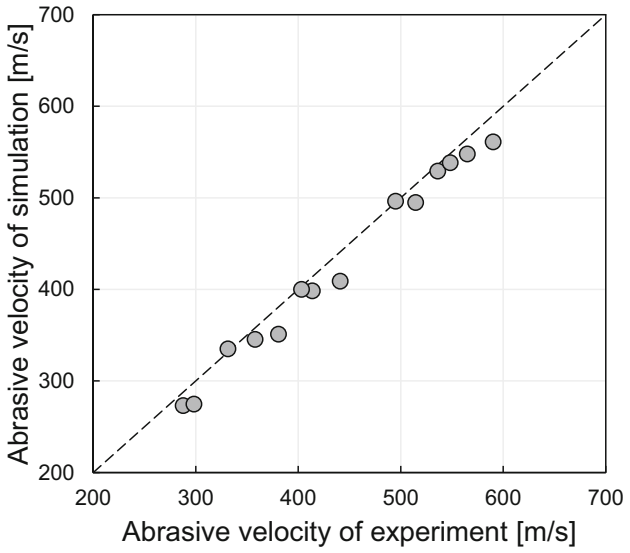

Fig. 5 Comparison of abrasive velocity between experimental test [3] and numerical simulation (this study)

4 Results and discussion

4.1 Effect of abrasive flow rate

Figure 6a shows the results of the numerical simulations used to analyze the effect of the abrasive flow rate on the abrasive velocity. The abrasive velocity (v_a) decreases as the abrasive flow rate ($\dot{m}_a$) increases. When a constant pump pressure is applied, the water has the same momentum as a waterjet system with a constant orifice diameter. When the water is mixed with the abrasive, the momentum of water is transmitted to the abrasive according to the law of conservation of momentum. Therefore, as the abrasive flow rate increases, the abrasive velocity (v_a) of each abrasive particle sprayed from the tip of the focusing tube decreases.

When there is no energy loss in the process of transferring the momentum of water to the abrasive, the abrasive velocity (v_a) is represented by the dotted line in Fig. 6a, according to the abrasive flow rate ($\dot{m}_a$). This is theoretically an ideal result, and it can be considered the maximum velocity of the abrasive that is generated when the momentum of the water is completely transferred to the abrasive (i.e., $v_{a,max}$). The velocity of the abrasive produced in the waterjet system is smaller than $v_{a,max}$ because of the energy loss due to collisions with the inner wall of the waterjet system. Figure 6b shows the difference between $v_{a,max}$ and the abrasive velocity (v_a) obtained through numerical analysis. As the abrasive flow rate ($\dot{m}_a$) increased, the values of $v_{a,max} - v_a$ decreased. This is because, as the abrasive flow rate increases, the abrasive particles align relatively quickly in the fluid and become straight, resulting in fewer collisions with the inner wall. Because the energy loss is less than that when the abrasive flow rate is relatively small, the value of $v_{a,max} - v_a$ decreases.

4.2 Effect of focusing tube geometry

Figure 7 shows the results of the numerical analysis of the effect of the focusing tube geometry on the abrasive velocity. The focusing tube geometry comprises two major parameters: the focusing tube diameter (D_f) and the focusing tube length (L_f). The abrasive velocity depends on the amount of energy that the abrasive loses as it passes through the focusing tube. As shown in Fig. 7a, the abrasive velocity increased as the focusing tube diameter increased, because under the same abrasive flow rate, as the focusing tube diameter increases, the distance between the abrasive and the inner wall increases, and thus, the number of collisions between the abrasive and wall decreases. However, it was confirmed that the effect of the focusing tube diameter on the abrasive velocity was insignificant under an abrasive flow rate condition of 15.0 g/s or higher because a larger abrasive flow rate results in faster alignment within the focusing tube; thus, the

Table 2 Simulation cases and details

Water pump pressure (MPa)	320						
Orifice diameter (mm)	0.15						
Water flow rate (ml/s)	10.67						
Abrasive flow rate (g/s)	Effect of abrasive flow rate						
	3.3	7.0	10.0	15.0	20.0	25.0	29.0
Focusing tube diameter (mm)	Effect of focusing tube diameter ($L_f = 76.2$ mm)						
	0.76	0.91	1.02				
Focusing tube length (mm)	Effect of focusing tube length ($D_f = 1.02$ mm)						
	76.2	101.6	152.4				

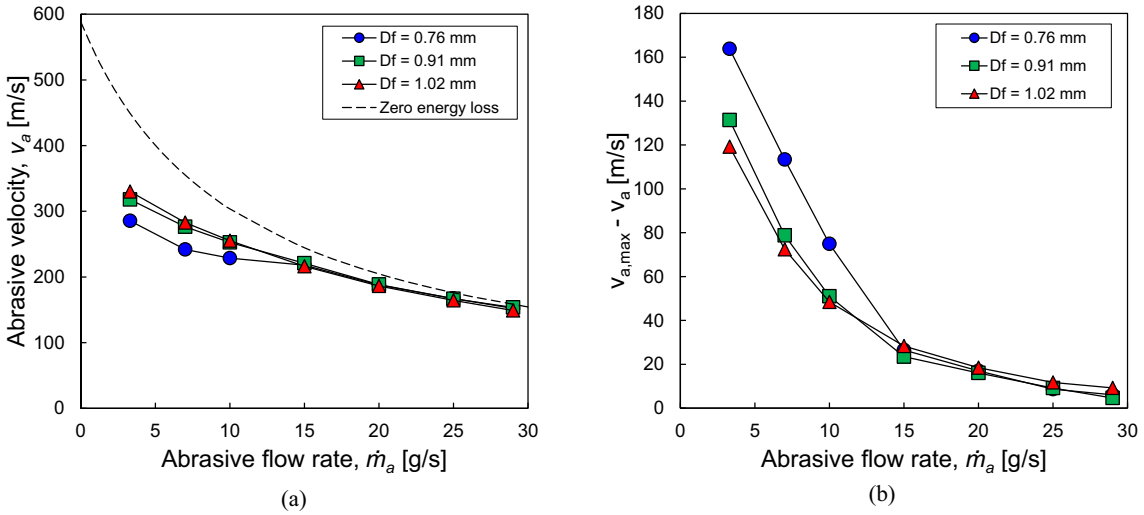

Fig. 6 Effect of abrasive flow rate on the abrasive velocity: **a** numerical simulation results and **b** difference between theoretical and numerical values

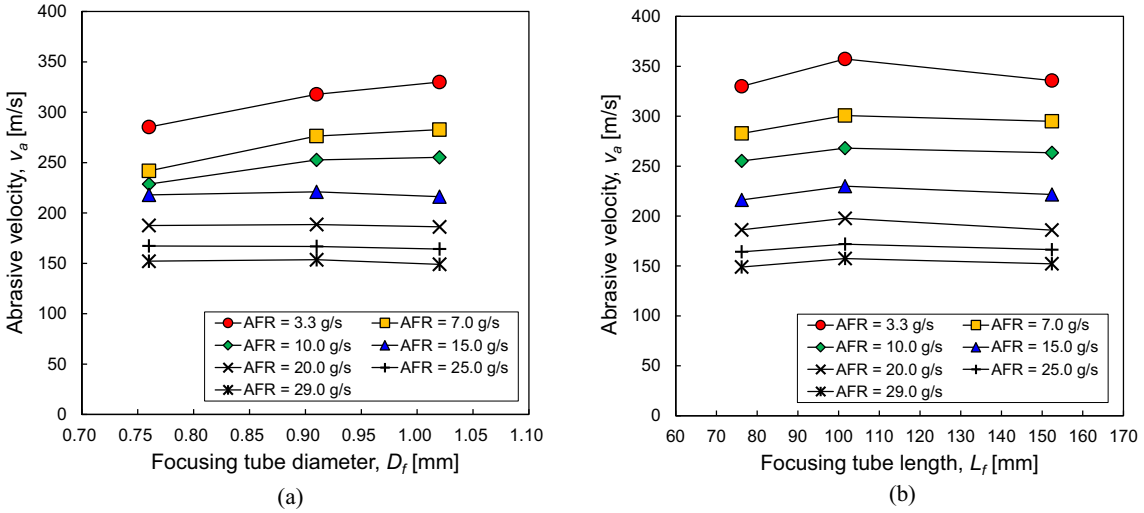

Fig. 7 Abrasive velocity on the focusing tube geometry: **a** focusing tube diameter and **b** focusing tube length

collision with the focusing tube wall is also reduced. Therefore, the effect on the focusing tube diameter was relatively reduced.

The effect of the focusing tube length on the abrasive velocity at the tip of the focusing tube was derived, as shown in Fig. 7b. A longer focusing tube length implies more time for the abrasive to pass through the focusing tube. As the time of traversal through the focusing tube increases, the number of collisions between the abrasive and the wall increases. Therefore, as the energy loss of the abrasive increases, the abrasive velocity is expected to decrease. However, according to the results of this numerical analysis, the abrasive velocity increased and then decreased as the focusing tube length increased for all abrasive flow rates. This result shows that the optimal focusing tube length exists to maximize the abrasive velocity when sprayed into air.

4.3 Momentum transfer efficiency

MTE is an index of how efficiently the momentum of water is transferred and imparts acceleration to the abrasive in an AWJ system. The abrasive velocity at the tip of the focusing tube is influenced and can be changed by adjusting various parameters (e.g., abrasive flow rate, focusing tube geometry, and water stiffness). As these parameters eventually affect the MTE, the MTE characteristics considering abrasive flow rate, focusing tube geometry, and water stiffness are discussed in this section.

The effect of the abrasive flow rate (AFR) on the MTE was obtained as shown in Fig. 8a. As the AFR increased, the MTE increased and converged. As the MTE approaches 1, the momentum of water is transmitted to the abrasive with only a marginal loss of energy. However, a large AFR input

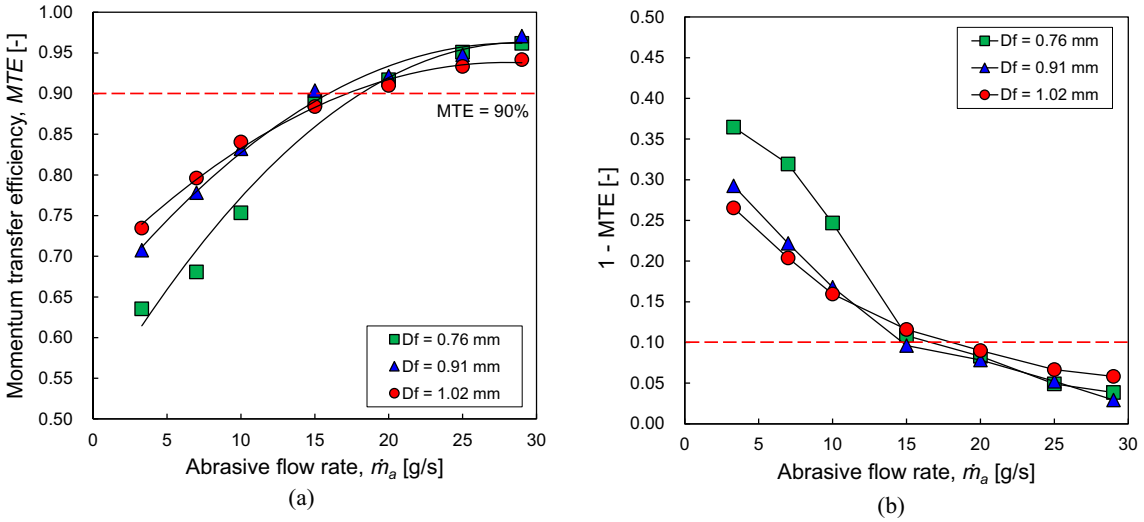

Fig. 8 Effect of abrasive flow rate on the momentum transfer efficiency: **a** numerical simulation results and **b** difference between theoretical and numerical values

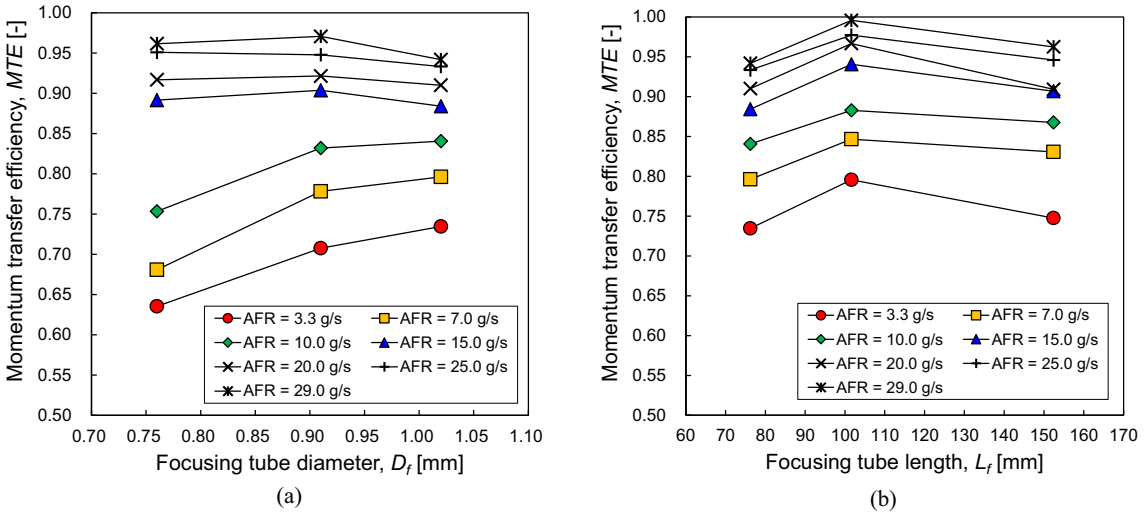

Fig. 9 Momentum transfer efficiency on the focusing tube geometry: **a** focusing tube diameter and **b** focusing tube length

to obtain an MTE close to 1 is economically disadvantageous. As shown in Fig. 8b, when the AFR = 15 g/s, which is approximately twice as large as the AFR of 7 g/s, the MTE increased by approximately 25%. However, when AFR = 29 g/s, which is approximately twice that of 15 g/s, the MTE increased by only 5%. Therefore, if the input AFR $\geq$ 15 g/s, the acceleration transfer to the abrasive becomes inefficient. It is necessary to generate an effective MTE by inputting a reasonable AFR when applied to rock excavation using an AWJ.

The effect of the focusing tube geometry on the MTE is shown in Fig. 9. The effect of the focusing tube diameter on the MTE can be clearly observed in Fig. 9a. As the focusing tube diameter increased, the MTE increased under a low AFR ($\dot{m}_a$ < 15.0 g/s). On the contrary, at a high AFR ($\dot{m}_a \geq$ 15.0 g/s), the effect of the focusing tube diameter on the MTE was insignificant. This can be attributed to the relatively higher collision frequency between the abrasive and the focusing tube wall than between the abrasives under low AFR ($\dot{m}_a$ < 15.0 g/s). In other words, there was little change in the acceleration efficiency of abrasive particles depending on the focusing tube diameter under the high AFR. Meanwhile, a large focusing tube diameter was advantageous in accelerating abrasive particles under the low AFR. In conclusion, there is an optimal combination of focusing tube diameter and AFR for MTE, and in order to create an efficient MTE, the use of a large focusing tube diameter is recommended regardless of the AFR condition. Figure 9b shows the effect of the focusing tube length on the MTE. In all the AFR cases, the MTE increased and decreased as the

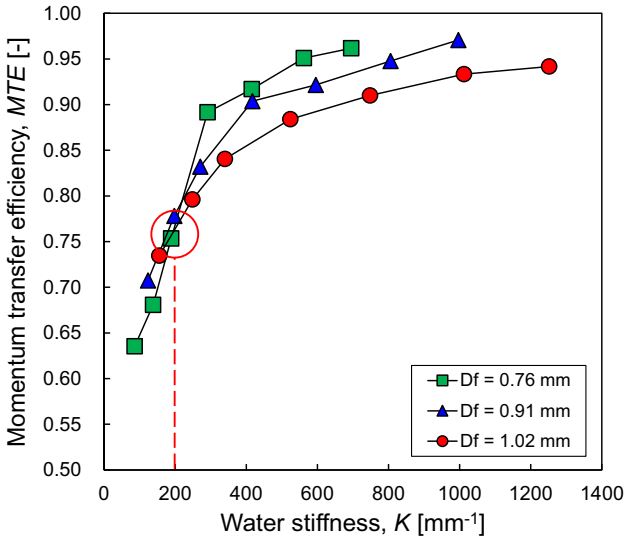

Fig. 10 Effect of water stiffness on the momentum transfer efficiency

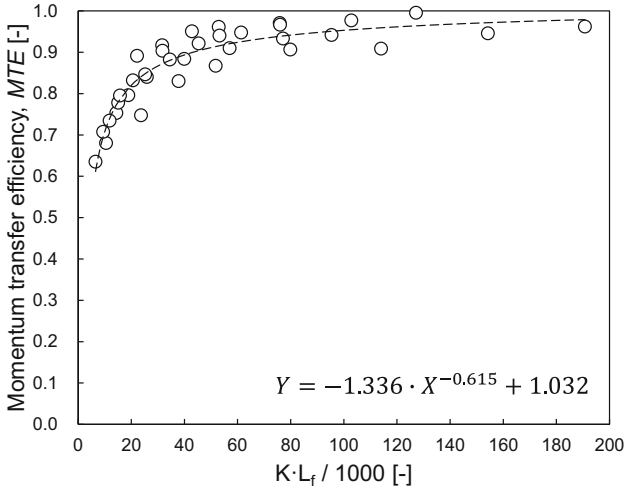

Fig. 11 Momentum transfer efficiency as a function of water stiffness and focusing tube length

focusing tube length increased. Figure 9b is the result under the condition that the focusing tube diameter is 1.02 mm, and shows that the optimal combination between focusing tube diameter and focusing tube length exists. Therefore, in order to generate an effective MTE, the optimal focusing tube length must also be determined depending on the focusing tube diameter.

Figure 10 shows the effect of water stiffness on the MTE. The water stiffness is affected by various parameters (e.g., drag coefficient, abrasive flow rate, water flow rate, orifice diameter, focusing tube diameter, and abrasive size). For all focusing tube diameters, as the water stiffness increased, the MTE increased, showing a gradual convergence. In addition, for a specific water stiffness ($K = 200$ mm^{-1}), the MTE exhibited crossed results according to the focusing tube diameter. When the water stiffness is below 200 mm^{-1}, a larger focusing tube diameter is more advantageous because it forms a large MTE. On the other hand, when the water stiffness is above 200 mm^{-1}, a smaller focusing tube diameter is more advantageous because it forms a large MTE. It is possible to obtain an optimal combination of focusing tube diameter and water stiffness for effective MTE. Therefore, it is possible to design an optimal AWJ system.

4.4 Prediction model of abrasive particle velocity

MTE exhibits different characteristics depending on various parameters (e.g., water stiffness, focusing tube length, etc.). To derive a reasonable MTE, it is necessary to understand the optimal conditions of these parameters. Figure 11 clearly shows the relationship between the water stiffness and focusing tube length for the MTE. The properties of the water stiffness and focusing tube length for the MTE are correlated with $= -1.336$, $\beta = -0.615$, and $\gamma = 1.032$, which can be expressed as follows:

$$MTE = -1.336 \cdot \left(\frac{K \cdot L_f}{1000} \right)^{-0.615} + 1.032. \tag{5.1}$$

In conclusion, by substituting Eqs. (2.3) and (5.1) into Eq. (2.8), the prediction model of abrasive velocity at the tip of the focusing tube can be written as:

$$\therefore v_a = \frac{C_d \cdot \psi}{1 + \dot{m}_a/\dot{m}_w} \sqrt{\frac{2 \cdot p_{w,p}}{\rho_w}} \cdot \left[-\left(\frac{2136 \cdot D_o^2/D_f^2 \cdot D_a}{C_D \cdot L_f \cdot (1 + \dot{m}_a/\dot{m}_w)^2} \right)^{0.615} + 1.032 \right]. \tag{5.2}$$

4.5 Parametric study

A parametric study was performed using the final derived prediction model of the abrasive velocity. The effects of two major ratios on the abrasive velocity were investigated (i.e., abrasive–water flow ratio and focusing tube geometry ratio). This parameter can be set according to the purpose of excavation performance when an AWJ system is applied to rock excavation.

Figure 12 shows the effect of the abrasive–water flow ratio ($\dot{m}_a/\dot{m}_w$) on the abrasive velocity (v_a). When the abrasive–water flow ratio was approximately 0.83, the abrasive velocity at the tip of the focusing tube was at its maximum value, which is the optimal mass flow ratio of the water and abrasives. In addition, when the abrasive–water flow ratio was below 0.83, the abrasive velocity increased with a steep

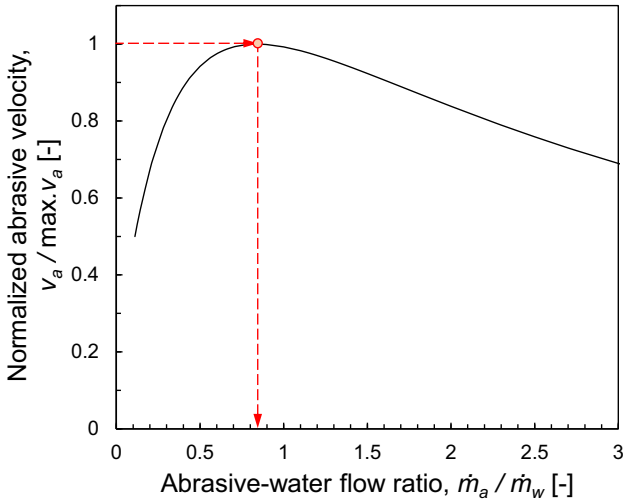

Fig. 12 Effect of abrasive–water flow ratio on the normalized abrasive velocity

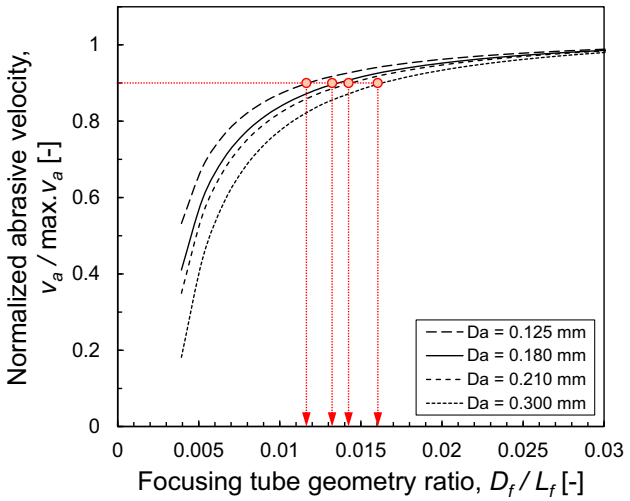

Fig. 13 Effect of focusing tube geometry ratio on the normalized abrasive velocity

slope. Contrarily, when the abrasive–water flow ratio was above 0.83, the abrasive velocity decreased with a relatively small slope. The abrasive velocity exhibited a more sensitive change when the abrasive–water flow ratio was insufficient ($\dot{m}_a/\dot{m}_w < 0.83$).

The effect of the focusing tube geometry ratio (D_f/L_f) on the abrasive velocity (v_a) at the tip of the focusing tube according to the abrasive diameter (D_a) is shown in Fig. 13. As the focusing tube geometry ratio increased, the abrasive velocity increased and converged, because as the focusing tube geometry ratio increases, the distance between the abrasive and the focusing tube wall increases, and thus, the energy dissipation due to collision is relatively reduced [6]. In addition, under the same focusing tube geometry ratio, as the abrasive diameter increased, the abrasive velocity at the end of the focusing tube decreased, because as the abrasive diameter increases, the mass to be accelerated by the momentum transfer from the water increases. In addition, we analyzed the required focusing tube geometry ratio when the normalized abrasive velocity was 0.9 in terms of the acceleration efficiency of the abrasive. When the abrasive diameter (D_a) was 0.125, 0.18, 0.21, and 0.30, the required focusing tube geometry ratio were approximately 0.012, 0.013, 0.014, and 0.016, respectively. In conclusion, as the abrasive diameter increased, a larger focusing tube geometry ratio was required to generate a velocity corresponding to 90% of the maximum abrasive velocity.

5 Conclusions

This study aimed to derive the abrasive velocity for an optimal system design in rock excavation using an AWJ. The abrasive velocity was numerically analyzed based on the operating parameters. To evaluate the comprehensive effects of the operating parameters, the MTE was defined and analyzed. In addition, the MTE was empirically expressed as a function of the operating parameters. From the results, a prediction model for the abrasive velocity was derived through theoretical and numerical approaches. The results and considerations are summarized as follows:

- A numerical simulation was performed by implementing a three-dimensional AWJ model of three-phase flow (i.e., air–water–abrasive) based on the Eulerian–Lagrangian approach. The model was validated by comparing it with the experimental results for the abrasive velocity at the tip of the focusing tube.
- A numerical analysis of the AWJ system was performed for the operating parameters (e.g., abrasive flow rate, focusing tube diameter, and focusing tube length). The abrasive velocity at the tip of the focusing tube was observed, and the comprehensive effects among the operating parameters were evaluated. The abrasive velocity increased as the abrasive flow rate decreased and the focusing tube diameter increased. In addition, as the focusing tube length increased, the abrasive velocity first increased and then decreased, exhibiting a maximum value.
- The effects of AFR, focusing tube diameter, focusing tube length, and water stiffness on the MTE were evaluated. The MTE increased as the AFR, focusing tube diameter, and water stiffness increased. However, as the focusing tube length increased, the MTE increased and then decreased, and a local maximum was observed.
- The MTE was derived from an empirical equation based on a comprehensive analysis of the abrasive flow rate, focusing tube geometry (i.e., diameter and length), and water

stiffness. In addition, an abrasive velocity prediction model that considers the operating parameters under comprehensive conditions was proposed using the derived empirical equation of the MTE.

- A parametric study was performed using the proposed prediction model of abrasive velocity, and an optimal abrasive velocity could be derived when an abrasive–water flow ratio of 0.83 was applied to the AWJ system. In addition, as the abrasive diameter increased, a larger focusing tube geometry ratio was required to generate the optimal abrasive velocity.

For future studies, the abrasive velocity at the tip of the focusing tube can be numerically investigated for abrasive particle characteristics such as size distribution, density, etc. Furthermore, a modified model considering abrasive particle characteristics can be proposed based on various approaches.

Acknowledgements This work was supported by the National Research Foundation of Korea (NRF) grant funded by the Korea government (MSIT) (No. 2017R1A5A1014883) and a Grant (RS-2023-00245334) funded by Korea of Ministry of Land, Infrastructure and Transport (MOLIT) and with technical support from ANSYS Korea.

Funding Open Access funding enabled and organized by KAIST.

Declarations

Conflict of interest The authors declare that they have no conflicts of interest.

References

1. Akkurt A (2009) The effect of material type and plate thickness on drilling time of abrasive water jet drilling process. Mater Des 30(3):810–815
2. Aydin G, Karakurt I, Amiri MR, Kaya S (2022) Improvement of rock cutting performance through two-pass abrasive waterjet cutting. Sustainability 14(19):12704
3. Balz R, Mokso R, Narayanan C, Weiss DA, Heiniger KC (2013) Ultra-fast X-ray particle velocimetry measurements within an abrasive water jet. Exp Fluids 54(3):1–13
4. Bridgman PW (1970) The physics of high pressure, 1st edn. Dover Publications Inc, New York
5. Cha Y, Oh TM, Cho GC (2019) Waterjet erosion model for rock-like material considering properties of abrasive and target materials. Appl Sci 9(20):4234
6. Cha Y, Oh TM, Cho GC (2020) Effects of focus geometry on the hard rock-cutting performance of an abrasive waterjet. Adv Civ Eng 2020:1–13
7. Cha Y, Oh TM, Joo GW, Cho GC (2021) Performance and reuse of steel shot in abrasive waterjet cutting of granite. Rock Mech Rock Eng 54(3):1551–1563
8. Cha Y, Oh TM, Hwang HJ, Cho GC (2021) Simple approach for evaluation of abrasive mixing efficiency for abrasive waterjet rock cutting. Appl Sci 11(4):1543
9. Chalmers EJ (1991) Effect of parameter selection on abrasive waterjet performance. In: Proceeding of the American water jet conference, Houston, USA, Paper. Vol. 25
10. Deepak D, Anjaiah D, Karanth KV, Sharma NY (2012) CFD simulation of flow in an abrasive water suspension jet: the effect of inlet operating pressure and volume fraction on skin friction and exit kinetic energy. Adv Mech Eng 4:186430
11. Du M, Wang H, Dong H, Guo Y, Ke Y (2021) Numerical research on multi-particle movements and nozzle wear involved in abrasive waterjet machining. Int J Adv Manuf Technol 117(9):2845–2858
12. Engin IC, Bayram F, Yasitli NE (2013) Experimental and statistical evaluation of cutting methods in relation to specific energy and rock properties. Rock Mech Rock Eng 46(4):755–766
13. Finnie I (1960) Erosion of surfaces by solid particles. Wear 3(2):87–103
14. Fluent ANSYS (2021) ANSYS Fluent 2021 R1 user's guide and theory manual. ANSYS Inc., USA
15. Gryc R, Hlaváč LM, Mikoláš M, Šancer J, Daněk T (2014) Correlation of pure and abrasive water jet cutting of rocks. Int J Rock Mech Min Sci 65:149–152
16. Guha A, Barron RM, Balachandar R (2011) An experimental and numerical study of water jet cleaning process. J Mater Process Technol 211(4):610–618
17. Hashish M (1989) Pressure effects in abrasive-waterjet (AWJ) machining. J Eng Mater Technol 111(3):221–228
18. Hashish M (1991) Optimization factors in abrasive-waterjet machining. J Eng Ind 113(1):29–37
19. Hashish M (2003) Inside AWJ nozzles. In: Proceedings of the 2003 American WJTA Conference, Houston, Texas
20. Hashish M (1984) A modeling study of metal cutting with abrasive waterjets. J Eng Mater Technol 106(1):88–100
21. Hirt CW, Nichols BD (1981) Volume of fluid (VOF) method for the dynamics of free boundaries. J Comput Phys 39(1):201–225
22. Hou R, Huang C, Zhu H (2013) Numerical simulation of multiphase flow field in abrasive waterjet machining. Int J Abras Technol 6(1):40–57
23. Hu G, Zhu W, Yu T, Yuan J (2008) Numerical simulation and experimental study of liquid-solid two-phase flow in nozzle of DIA jet. In: 2008 6th IEEE international conference on industrial informatics. pp. 1700–1705. IEEE.
24. Huang CZ, Hou RG, Wang J, Feng YX (2006) The effect of high pressure abrasive water jet cutting parameters on cutting performance of granite. Key Eng Mater 304:560–564
25. Jegaraj JJR, Babu NR (2007) A soft computing approach for controlling the quality of cut with abrasive waterjet cutting system experiencing orifice and focusing tube wear. J Mater Process Technol 185(1–3):217–227
26. Karakurt I, Aydin G, Aydiner K (2010) Effect of the abrasive grain size on the cutting performance of concrete in AWJ technology. Technology 13(3):145–150
27. Kaya S, Aydin G, Karakurt I (2023) An experimental study on the cutting depth produced by abrasive waterjet: how do abrasive and rock properties affect the cutting process? Int J Adv Manuf Technol 125(9–10):4811–4823

28. Kechagias J, Petropoulos G, Vaxevanidis N (2012) Application of Taguchi design for quality characterization of abrasive water jet machining of TRIP sheet steels. Int J Adv Manuf Technol 62(5):635–643
29. Korat MM, Acharya GD (2014) A review on current research and development in abrasive waterjet machining. Int J Eng Res Appl 4(1):423–432
30. Launder BE, Spalding DB (1983) The numerical computation of turbulent flows. In: Numerical prediction of flow, heat transfer, turbulence and combustion. pp. 96–116. Pergamon
31. Liu H, Wang J, Kelson N, Brown RJ (2004) A study of abrasive waterjet characteristics by CFD simulation. J Mater Process Technol 153:488–493
32. Long X, Liu Q (2018) Numerical analysis of the liquid-gas-solid three phase flow inside AWJ nozzle. In: Abrasive technology-characteristics and applications. IntechOpen
33. Long X, Ruan X, Liu Q, Chen Z, Xue S, Wu Z (2017) Numerical investigation on the internal flow and the particle movement in the abrasive waterjet nozzle. Powder Technol 314:635–640
34. Miller D (2004) Fluid dynamics of abrasive waterjet cutting heads. In: Proceedings of the 17th international conference on water jetting, Cranfield, Mainz, Germany, BHR Group Limited. pp. 107–121
35. Momber AW (2001) Energy transfer during the mixing of air and solid particles into a high-speed waterjet: an impact-force study. Exp Thermal Fluid Sci 25(1–2):31–41
36. Momber AW (2004) Wear of rocks by water flow. Int J Rock Mech Min Sci 41(1):51–68
37. Momber AW, Kovacevic R (1995) Energy dissipative processes in high speed water-solid particle erosion. Asme-Publ-Htd 321:555–564
38. Momber AW, Kovacevic R (1997) Test parameter analysis in abrasive water jet cutting of rocklike materials. Int J Rock Mech Min Sci 34(1):17–25
39. Momber AW, Kovacevic R (1998) Principles of abrasive water jet machining. Springer, Berlin
40. Mostofa MG, Kil KY, Hwan AJ (2010) Computational fluid analysis of abrasive waterjet cutting head. J Mech Sci Technol 24(1):249–252
41. Nambiath P, Galecki G, Summers DA (2007) Energy based modelling of abrasive slurry jet. In: Proceeding of the 2007 American water jet conference, Texas, Paper
42. Nyaboro JN, Ahmed MA, El-Hofy H, El-Hofy M (2018) Numerical and experimental characterization of kerf formation in abrasive waterjet machining. In: ASME international mechanical engineering congress and exposition. Vol. 52019, p. V002T02A050. American Society of Mechanical Engineers
43. Oh TM, Cho GC (2014) Characterization of effective parameters in abrasive waterjet rock cutting. Rock Mech Rock Eng 47(2):745–756
44. Oh TM, Joo GW, Cho GC (2019) Effect of abrasive feed rate on rock cutting performance of abrasive waterjet. Rock Mech Rock Eng 52(9):3431–3442
45. Prisco U, D'Onofrio MC (2008) Three-dimensional CFD simulation of two-phase flow inside the abrasive water jet cutting head. Int J Comput Methods Eng Sci Mech 9(5):300–319
46. Qiang Z, Wu M, Miao X, Sawhney R (2018) CFD research on particle movement and nozzle wear in the abrasive water jet cutting head. Int J Adv Manuf Technol 95(9):4091–4100
47. Roth P, Looser H, Heiniger KC, Bühler S (2005) Determination of abrasive particle velocity using laser-induced fluorescence and particle tracking methods in abrasive water jets. In: Proceedings of 2005 WJTA Conference and exposition. pp. 21–23
48. Summers DA (1995) Waterjetting technology. CRC Press, Boca Raton
49. Tazibt A, Parsy F, Abriak N (1996) Theoretical analysis of the particle acceleration process in abrasive water jet cutting. Comput Mater Sci 5(1–3):243–254
50. Wang J (2009) Particle velocity models for ultra-high pressure abrasive waterjets. J Mater Process Technol 209(9):4573–4577
51. Wang R, Wang M (2010) A two-fluid model of abrasive waterjet. J Mater Process Technol 210(1):190–196